Supplemental Material

Chemicals. Anhydrous copper(II) fluoride (Aldrich, 98%), pyrazine (Aldrich, 99%), and 4,4'-dipyridyl (Aldrich 98%) were used as received.

Synthesis of CuF_2(pyz) by use of high pressure. Equimolar amounts of anhydrous copper(II) fluoride and pyrazine were ground into a powder and packed into a capsule made of gold foil. These capsules have a height of 0.375", an inside diameter of 0.181", and a wall thickness of 0.002". This sample capsule was then compacted with 1 ton of force through use of a Carver laboratory press. The compacted sample capsule was placed inside an alumina ceramic sleeve which was further slid inside a graphite tube that acts as a heater. Bisque fired alumina disks were placed above and below the sample can. The entire assembly was then placed inside a pyrophyllite cube fitted with a thermocouple. This entire assembly was placed inside a Rockland Research high pressure synthesis press apparatus. The pressure was gradually increased to about 4 GPa over a period of about 3 hours. A voltage was then applied across the graphite heater to provide a temperature of about 100 °C. The reaction occurred under these conditions over a period of 3-12 hours. The temperature was returned to ambient over a period of about 1 minute and the pressure returned to ambient overnight.

Synthesis of CuF_2(pyz) by thermal annealing. Anhydrous copper(II) fluoride (20 mmol, 2030 mg) and pyrazine (20 mmol, 1600 mg) were ground into a powder and placed in a 23 ml Teflon cup and loaded into a Parr General Purpose Acid Digestion Bomb (Model 4744). The bomb was then placed in a Fisher Scientific Isotemp Oven and heated at 100 °C for a period of 2-4 weeks. During this period, the sample was cooled, reground, and returned to the oven about every five days.

Synthesis of $CuCl_2$(pyz) and $CuBr_2$(pyz). Pyrazine (2 mmol, 0.160 g, Aldrich) was dissolved in distilled water (10 ml). An aqueous solution (5 ml) of $CuCl_2 \cdot 2H_2O$ (1 mmol, 0.1795 g, Aldrich) was then added dropwise to the pyz solution. Green rod-like crystals of $CuCl_2$(pyz) were obtained by slow evaporation of water at room temperature over a period of one week. Anal. Calcd (%) for $C_4H_4Cl_2CuN_2$: C, 22.39; H, 1.88; Cl, 33.05; N, 13.06. Found: C, 22.59; H, 2.06; Cl, 32.91; N, 12.89. IR (cm^{-1}): 3117 w, 3111 w, 1482 w, 1413 s, 1281 m, 1165 s, 1113 s, 1092 m, 1065 s, 866 w, 802 vs. To obtain $CuBr_2$(pyz), the above procedure was applied, substituting $CuCl_2$ with $CuBr_2$ (1 mmol, 0.2224 g). Blocky red-brown crystals were recovered upon the evaporation of water at room temperature. Anal. Calcd (%) for $C_4H_4Br_2CuN_2$: C, 15.83; H, 1.33; Br, 52.66; N, 9.23. Found: C, 15.89; H, 1.35; Br, 52.78; N, 9.25. IR (cm^{-1}): 3111 w, 3102 w, 3055 w, 1483 m, 1412 vs, 1362 w, 1279 m, 1161 s, 1113 s, 1092 m, 1062 s, 966 w, 868 w, 796 vs.

Synthesis of CuF_2(44bpy) by thermal annealing. Anhydrous copper(II) fluoride (5 mmol, 507 mg) and 4,4'-dipyridyl (5 mmol, 781 mg) were ground into a powder and placed in a 23 ml Teflon cup and loaded into a Parr General Purpose Acid Digestion Bomb (Model 4744). The bomb was then placed in a Fisher Scientific Isotemp Oven and heated at 100 °C for a period of 4 days. The sample was returned to the oven and heated at 100 °C for a period of 11 days.

Infrared Spectroscopy. Infrared spectra were measured between 4000 and 750 cm^{-1} through use of a Bruker Vertex 70 spectrometer equipped with a PIKE Technologies MIRacle™ attenuated total reflectance (ATR) stage. For CuF_2(pyz) IR (cm^{-1}): 1414 w, 1392 w, 1177 m, 1104 m, 1080 m, 1064 vs, 829 s.

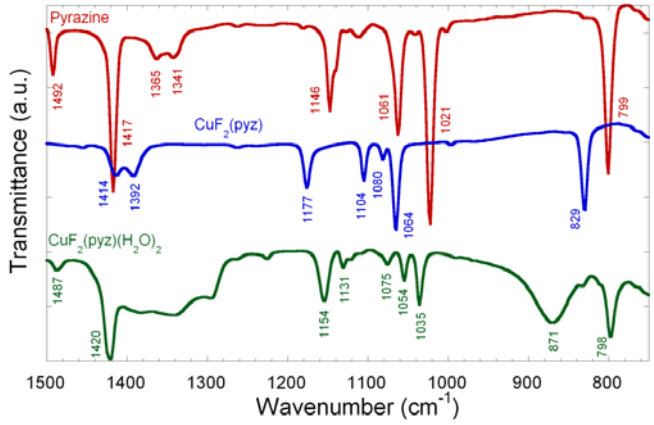

Fig. S1, Infrared spectrum of CuF_2(pyz) as compared to pyrazine and CuF_2(pyz)$(H_2O)_2$.

Thermogravimetric Analysis (TGA). Data were collected on a TA Instruments Q50 thermogravimetric analyzer in flowing nitrogen at a heating rate of 10 °C/min to a final temperature of 500 °C. A thermogravimetric analysis of $CuF_2(pyz)$ indicates a 43 % weight loss beginning near 250 °C, corresponding well with the theoretical value (44%) resulting from removal of the pyrazine ligand.

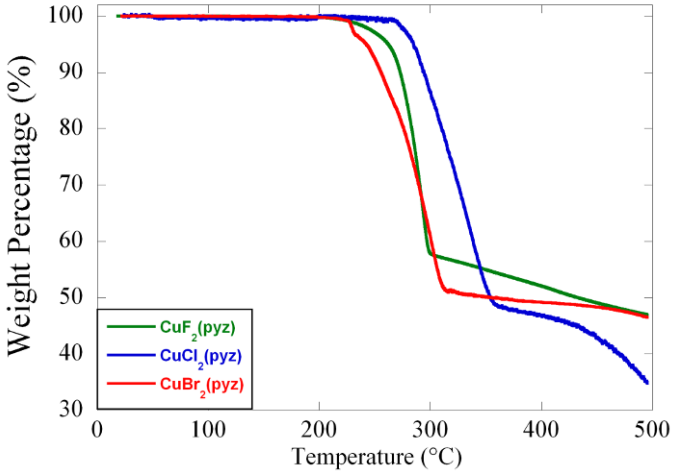

Fig. S2, Thermogravimetric analysis of $CuF_2(pyz)$ as compared to $CuCl_2(pyz)$ and $CuBr_2(pyz)$

Density Functional Theory. For evaluation of the exchange couplings, the broken-symmetry (BS) approach of Noodleman[1] as implemented in the ORCA ver. 2.8 suite of programs[2-4] was employed. The formalism of Yamaguchi, which employs calculated expectation values $\langle S^2 \rangle$ for both high-spin and broken-symmetry states was used.[5, 6] Calculations related to magnetic interactions have been performed using the PBE0 functional. The def2-TZVP basis function set from Alrichs was used.[7] Spin densities were visualized using the UCSF Chimera program ver. 1.5.3. SCF convergence of the BS state of the 4,4'-bipyridine-bridged model required tighter integration grid (keyword: GRID7) and use of approximate second order SCF (keyword: SOSCF). Convergence criteria were identical for the both chemical models.

The magnetic exchange in $CuF_2(pyz)$ was modeled by dinuclear fragments encompassing either fluoride or pyrazine bridging, based on atomic coordinates obtained at 12 K. In order to demonstrate that the DFT calculations based on low temperature structures more accurately reflect the low temperature magnetic behavior, calculations were also performed based on the 100 K structure. Computed exchange coupling constants for model systems with the convention $H_{HDvV} = JS_1S_2$:

System	J / K
$[F_2Cu(pyz)_2(\mu\text{-}F)_2Cu(pyz)_2F_2]^{2-}$	0.63
$[F_4(pyz)Cu\ (\mu\text{-}pyz)CuF_4(pyz)]^{4-}$	11.6

As the crystal structure of $CuF_2(44bpy)$ is not available at 12 K, the magnetic exchange in this compound was modeled by dinuclear fragments encompassing either fluoride or 4,4'-bipyridine bridging, based on atomic coordinates obtained at 100 K. Computed exchange coupling constants for model systems with the convention $H_{HDvV} = JS_1S_2$:

System	J / K
$[F_2Cu(44bpy)_2(\mu\text{-}F)_2Cu(44bpy)_2F_2]^{2-}$	-0.89
$[\ F_4(44bpy)Cu\ (\mu\text{-}44bpy)CuF_4(44bpy)]^{4-}$	1.96

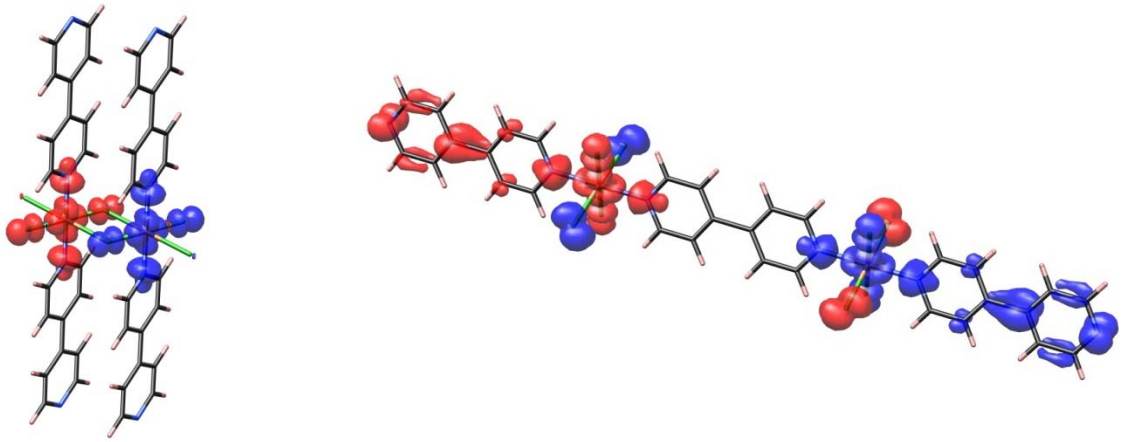

Fig. S3, Computed spin densities for the BS state of the dinuclear models examined for CuF2(44bpy). Plots are made with identical isosurface values of ±1.5E-3.

Magnetic Measurements. The variable-temperature dc magnetic susceptibility and the field dependence of magnetization were performed on a Quantum Design MPMS-7XL SQUID magnetometer equipped with a 70000 Oe superconducting magnet. Homogeneous powder samples were loaded into gelatin capsules and mounted on the end of a sample rod. The samples were cooled in zero-field to the lowest achievable temperature of 2 K, the magnet charged to field and data collected on warming to 300 K. The experimental susceptibilities were corrected for the diamagnetism of the constituent atoms. As $CuF_2(pyz)$ was prepared as a powder sample, we considered possible magnetic contamination from CuF_2[8-10] or $CuF_2(H_2O)_2$,[11, 12] but none was found. Pulsed-field magnetization measurements up to 25 T (rise/fall-time ~ 3 ms) were performed at the Nicholas Kurti Magnetic Field Laboratory in Oxford [$CuF_2(pyz)$] and up to 60 T (rise/fall-time ~ 10/50 ms) at the National High Magnetic Field in Los Alamos [$CuF_2(44bpy)$]. Powdered samples can be moved into and out of a 1500-turn, compensated-coil susceptometer, constructed from 25 μm high-purity copper wire. When the sample is within the coil and the field is pulsed the voltage induced in the coil is proportional to the rate of change of magnetization with time. Accurate values of the magnetization are then obtained by subtraction of the signal from that taken using an empty coil under the same conditions, followed by numerical integration. The susceptometer is placed inside a ^{3}He cryostat, which can attain temperatures as low as 0.5 K.

X-ray Powder Diffraction. Data for the structure solution of $CuF_2(pyz)$ and $CuF_2(44bipy)$ at 100K and 300K were collected through the mail-in program at Beamline 11-BM at the Advanced Photon Source at Argonne National Laboratory,[13] using an average wavelength of 0.413920 Å. Samples were loaded into kapton capillaries of a nominal 1mm diameter. Discrete detectors covering an angular range from -6 to 16 º 2θ are scanned over a 34º 2θ range, with data points collected every 0.001º 2θ and scan speed of 0.01º/s.

The 11-BM instrument uses x-ray optics with two platinum-striped mirrors and a double-crystal Si(111) monochromator, where the second crystal has an adjustable sagittal bend.[14] Ion chambers monitor incident flux. A vertical Huber 480 goniometer, equipped with a Heidenhain encoder, positions an analyzer system comprised of twelve perfect Si(111) analyzers and twelve Oxford-Danfysik LaCl3 scintillators, with a spacing of 2º 2θ.[15] Analyzer orientation can be adjusted individually on two axes. A three-axis translation stage holds the sample mounting and allows it to be spun, typically at ~5400 RPM (90 Hz). A Mitsubishi robotic arm is used to mount and dismount samples on the diffractometer. An Oxford Cryosystems Cryostream Plus device allows sample temperatures to be controlled over the range 80-500 K when the robot is used.

The diffractometer is controlled via EPICS.[16] Data are collected while continually scanning the diffractometer 2θ arm. A mixture of NIST standard reference materials, Si (SRM 640c) and Al2O3 (SRM 676) is used to calibrate the instrument, where the Si lattice constant determines the wavelength for each detector. Corrections are applied for detector sensitivity, 2θ offset, small differences in wavelength between detectors, and the source intensity, as noted by the ion chamber before merging the data into a single set of intensities evenly spaced in 2θ.

For the 12K $CuF_2(pyz)$, data was collected on a Panalytical XPert pro laboratory diffractometer, using Cu K_α radiation, with temperature control provided by an Oxford Phenix cryostat. The sample was placed on a zero background Si wafer and a small amount of Vaseline was mixed with the sample in order to improve thermal contact.

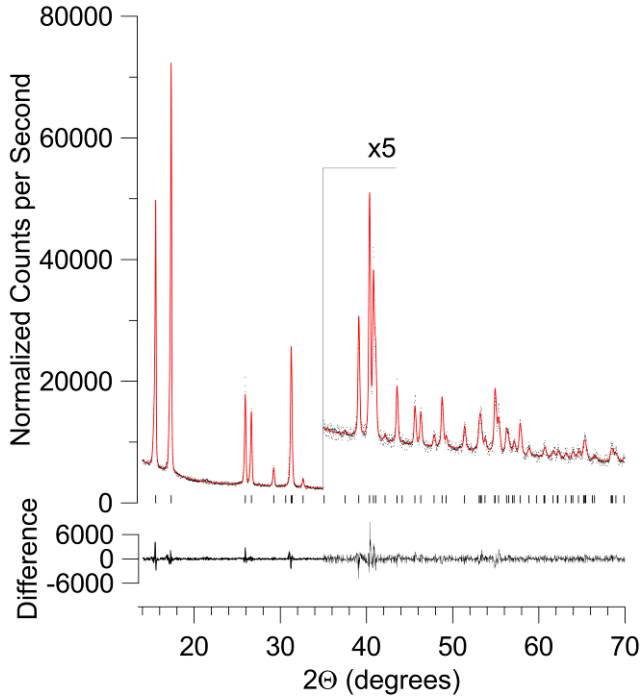

Fig S4. PXRD (dots) and Rietveld fit (line) of the data for $CuF_2(pyz)$ at 12K. The lower trace is the difference, measured – calculated, plotted to the same vertical scale.

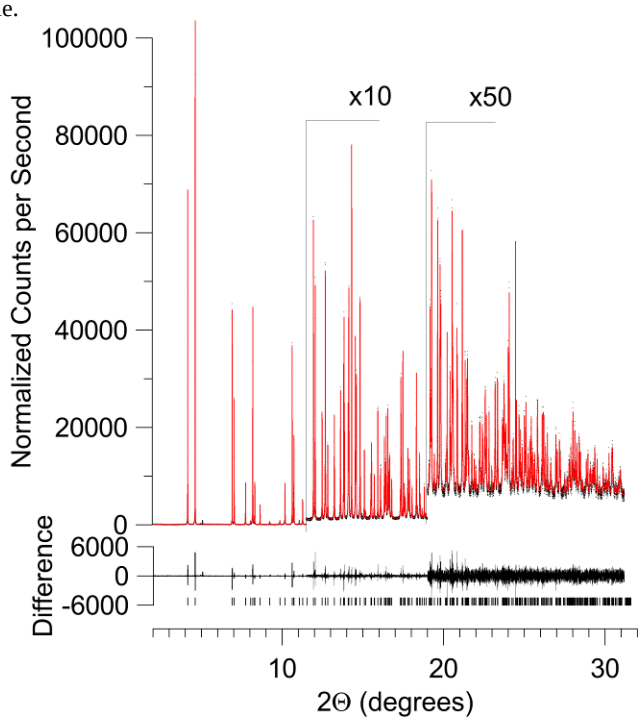

Fig S5. PXRD (dots) and Rietveld fit (line) of the data for $CuF_2(pyz)$ at 300K. The lower trace is the difference, measured – calculated, plotted to the same vertical scale.

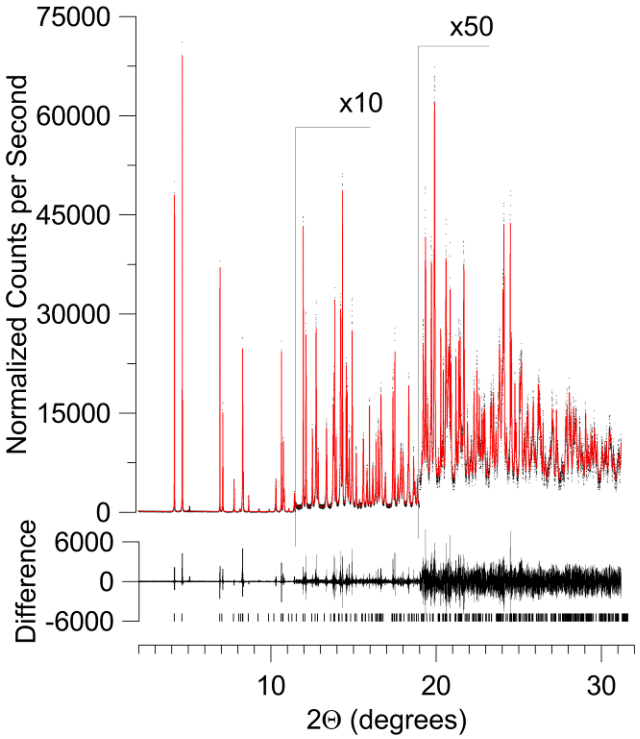

Fig S6. PXRD (dots) and Rietveld fit (line) of the data for CuF_2(pyz) at 100K. The lower trace is the difference, measured – calculated, plotted to the same vertical scale.

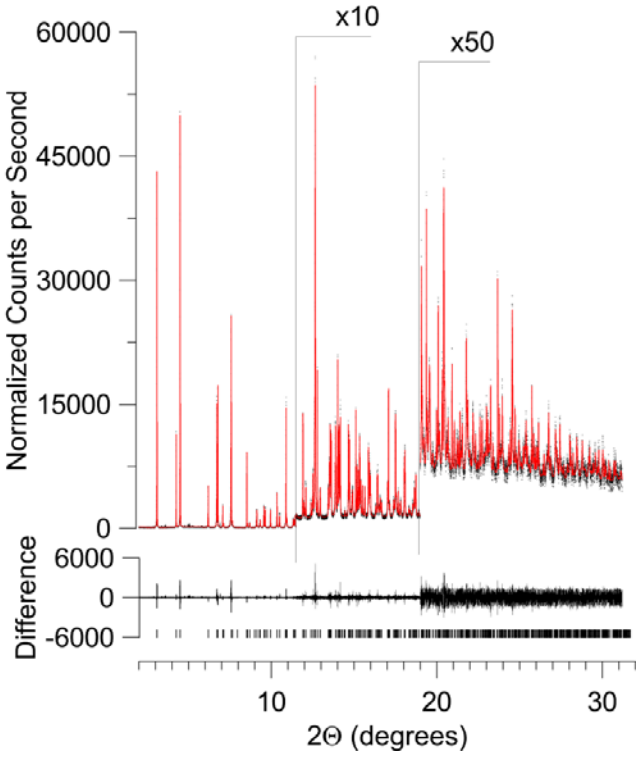

Fig S7. PXRD (dots) and Rietveld fit (line) of the data for CuF_2(44bipy) at 300K. The lower trace is the difference, measured – calculated, plotted to the same vertical scale.

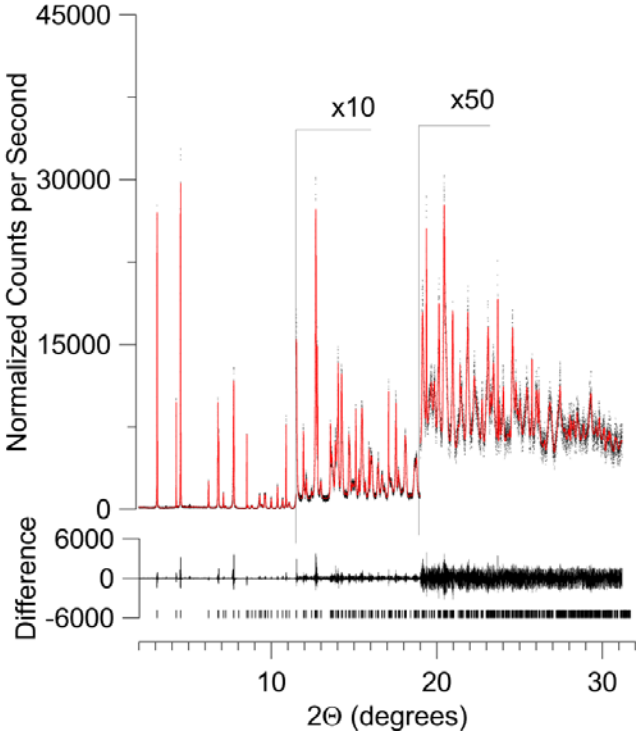

Fig S8. PXRD (dots) and Rietveld fit (line) of the data for CuF_2(44bipy) at 100K. The lower trace is the difference, measured – calculated, plotted to the same vertical scale.

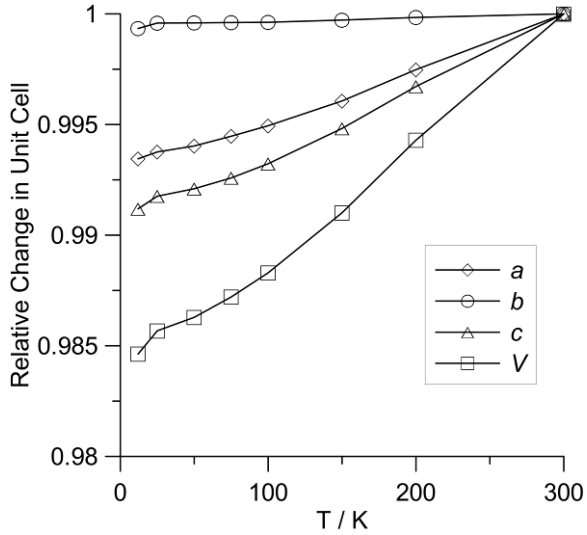

Fig. S9. Relative changes in unit cell dimensions for CuF_2(pyz) with temperature.

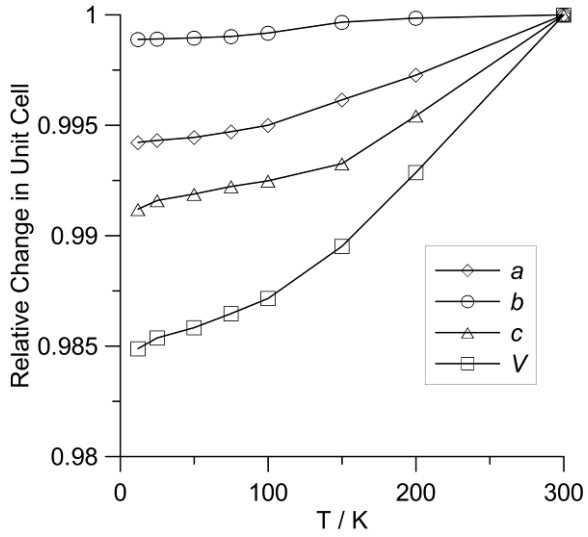

Fig S10. Relative changes in unit cell dimensions for $CuCl_2(pyz)$ with temperature.

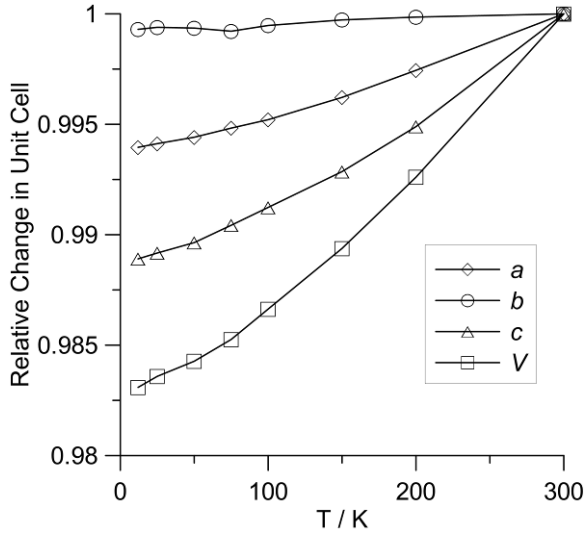

Fig. S11. Relative changes in unit cell dimensions for $CuBr_2(pyz)$ with temperature.

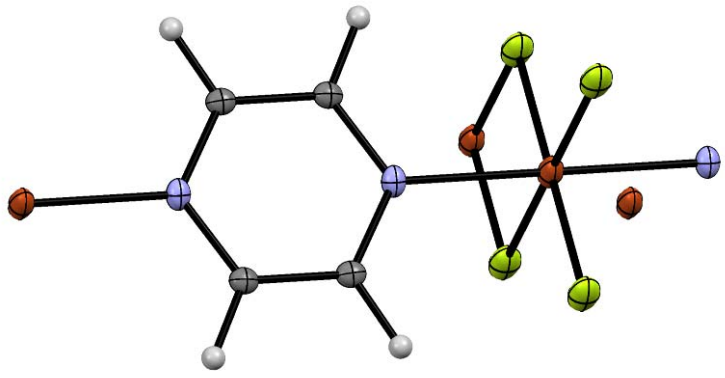

Fig. S12. Thermal ellipsoides for $CuF_2(pyz)$ at 100K. Thermal ellipsoids are drawn at the 50% probability level.

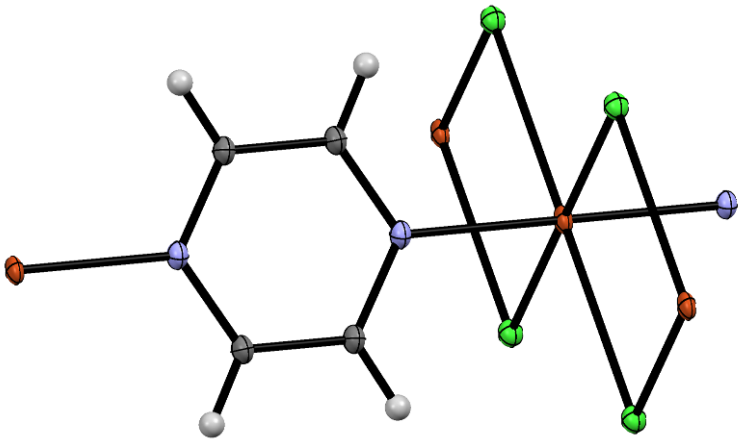

Fig. S13. Thermal ellipsoides for $CuCl_2(pyz)$ at 100K. Thermal ellipsoids are drawn at the 50% probability level.

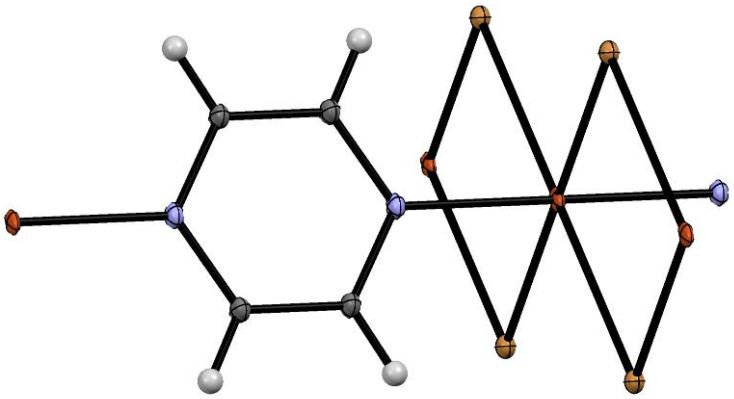

Fig. S14. Thermal ellipsoides for $CuBr_2(pyz)$ at 100K. Thermal ellipsoids are drawn at the 50% probability level.

Table 1. Crystal Data and Structure Refinement for CuX_2(L)

L	pyz							44bpy	
X	F			Cl		Br		F	
Formula	$CuF_2(C_4H_4N_2)$			$CuCl_2(C_4H_4N_2)$		$CuBr_2(C_4H_4N_2)$		$CuF_2(C_{10}H_8N_2)$	
M_W	181.62			214.53		303.45		257.72	
Crystal system	Monoclinic								
Space group	$C2/m$								
Method	Powder			Single Crystal		Single Crystal		Powder	
T/K	300(2)	100(2)	12(2)	300(2)	100(2)	300(2)	100(2)	300(2)	100(2)
a/Å	10.31147(2)	10.23657(4)	10.2346	11.9927(3)	11.9223(4)	12.4283(4)	12.3718(5)	10.65013(4)	10.57015(10)
b/Å	6.87249(1)	6.86371(2)	6.8659	6.8557(1)	6.8500(2)	6.8569(2)	6.8551(2)	11.14758(2)	11.14581(7)
c/Å	3.38094(1)	3.35108(1)	3.3473	3.7070(1)	3.6735(1)	3.9137(1)	3.8776(1)	3.56638(1)	3.50779(3)
β/°	93.38898(10)	92.7076(3)	92.627	95.935(1)	95.656(1)	96.340(1)	95.945(1)	97.4903(2)	96.6253(7)
V/Å^3	239.1733(6)	235.187(14)	234.967	303.150(12)	298.546(16)	331.48(2)	327.09(2)	419.799(2)	410.503(6)
Z	2								
D_c/ g cm^{-3}	2.522	2.565	2.567	2.350	2.386	3.040	3.081	2.039	2.085
μ/mm^{-1}	-	-	-	4.370	4.437	15.245	15.450	-	-
F(000)	-	-	-	210		282		-	-
R(int)	-	-	-	0.0158	0.0159	0.0274	0.0212	-	-
Total reflns	-	-	-	3362	3122	3661	3600	-	-
Unique reflns	-	-	-	547	536	590	591	-	-
$I > 2\sigma(I)$	-	-	-	541	535	581	586	-	-
$R(F_o)$	-	-	-	0.0160	0.0151	0.0163	0.0151	-	-
$R_w(F_o^2)$	-	-	-	0.450	0.0398	0.0418	0.0395	-	-
R_{wp}[1]	0.0766	0.1176	0.05185	-	-	-	-	0.0899	0.1072
R_{exp}	0.0481	0.0494	0.01725	-	-	-	-	0.0541	0.0543

[1] Higher than normal figures of merit are in part due to small impurities in the measured samples.

Table 2. Selected bond distances (Å) and angles (°) for CuX_2(*L*)

L	pyz							44bpy	
X	F			Cl		Br		F	
T/K	300(2)	100(2)	12(2)	300(2)	100(2)	300(2)	100(2)	300(2)	100(2)
				Bond distances (Å)					
Cu – *X*	1.889	1.899	1.920	2.2871(4)	2.2876(4)	2.4295(2)	2.4322(2)	1.898	1.911
Cu ··· *X*	2.497	2.453	2.432	2.8732(4)	2.8418(4)	3.0445(2)	3.0096(2)	2.742	2.622
Cu – N	2.046	2.035	2.072	2.0376(2)	2.0332(2)	2.038(2)	2.034(2)	2.027	2.028
				Bond Angles (°)					
Cu-*X*···Cu	99.96	99.92	99.71	91.11(1)	90.82(1)	90.56(1)	90.25(1)	98.84	100.22
X – Cu···*X*	80.04	80.08	80.29	88.89(1)	89.18(1)	89.44(1)	89.75(1)	81.16	79.78
				Cu-Cu Separations (Å)					
Cu-*X*···Cu (*c*)	3.38094(1)	3.35108(1)	3.3473	3.7070(1)	3.6735(1)	3.9137(1)	3.8776(1)	3.56713	3.5078
Cu-pyz-Cu (*b*)	6.87249(1)	6.86371(2)	6.8659	6.8557(1)	6.8500(2)	6.8569(2)	6.8551(2)	11.14809	11.146
				Torsion Angles (°)					
X-Cu-N-C	23.03	22.93	23.55	56.90(6)	57.18(5)	55.92(8)	55.51(8)	20.55	22.11

References:

1. L. Noodleman, *J. Chem. Phys.*, 1981, **74**, 5737-5743.
2. F. Neese, Institut für Physikalische und Theoretische Chemie, Universitaet Bonn, Germany., 2010.
3. F. Neese, *Coordination Chemistry Reviews*, 2009, **253**, 526-563.
4. S. Sinnecker, F. Neese and W. Lubitz, *J Biol Inorg Chem*, 2005, **10**, 231-238.
5. V. H. Smith, Schafer, F., III, Morokuma, K., Eds.; D. Reidel, ed. K. T. Yamaguchi, Y.; Fueno, T., Boston, MA, 1986, p. 155.
6. T. Soda, Y. Kitagawa, T. Onishi, Y. Takano, Y. Shigeta, H. Nagao, Y. Yoshioka and K. Yamaguchi, *Chemical Physics Letters*, 2000, **319**, 223-230.
7. F. Weigend and R. Ahlrichs, *Physical chemistry chemical physics : PCCP*, 2005, **7**, 3297-3305.
8. R. J. Joenk and R. M. Bozorth, *Journal of Applied Physics*, 1965, **36**, 1167-1168.
9. P. Fischer, W. Halg, D. Schwarzenbach and H. Gamsjager, *Journal of Physics and Chemistry of Solids*, 1974, **35**, 1683-1689.
10. P. Reinhardt, M. P. Habas, R. Dovesi, I. d. P. R. Moreira and F. Illas, *Physical Review B*, 1999, **59**, 1016-1023.
11. S. C. Abrahams, *Journal of Chemical Physics*, 1962, **36**, 56-61.
12. R. M. Bozorth and J. W. Nielsen, *Physical Review*, 1958, **110**, 879-880.
13. B. H. Toby, Y. Huang, D. Dohan, D. Carroll, X. S. Jiao, L. Ribaud, J. A. Doebbler, M. R. Suchomel, J. Wang, C. Preissner, D. Kline and T. M. Mooney, *Journal of Applied Crystallography*, 2009, **42**, 990-993.
14. J. Wang, B. H. Toby, P. L. Lee, L. Ribaud, S. M. Antao, C. Kurtz, M. Ramanathan, R. B. Von Dreele and M. A. Beno, *Review of Scientific Instruments*, 2008, **79**, 085105-085107.
15. P. L. Lee, D. Shu, M. Ramanathan, C. Preissner, J. Wang, M. A. Beno, R. B. Von Dreele, L. Ribaud, C. Kurtz, S. M. Antao, X. Jiao and B. H. Toby, *J Synchrotron Radiat*, 2008, **15**, 427-432.
16. L. R. Dalesio, J. O. Hill, M. Kraimer, S. Lewis, D. Murray, S. Hunt, W. Watson, M. Clausen and J. Dalesio, *Nucl Instrum Meth A*, 1994, **352**, 179-184.